# Decadal and Intra-Annual Variability of the Indian Ocean Freshwater Budget

KATHRYN L. GUNN,[a,b] K MCMONIGAL,[a,c] LISA M. BEAL,[a] AND SHANE ELIPOT[a]

[a] Rosenstiel School of Marine and Atmospheric Science, University of Miami, Miami, Florida
[b] Centre for Southern Hemisphere Oceans Research, CSIRO Oceans and Atmosphere, Hobart, Tasmania, Australia
[c] North Carolina State University, Raleigh, North Carolina

(Manuscript received 9 March 2022, in final form 11 May 2022)

ABSTRACT: The global freshwater cycle is intensifying: wet regions are prone to more rainfall, while dry regions experience more drought. Indian Ocean rim countries are especially vulnerable to these changes, but its oceanic freshwater budget—which records the basinwide balance between evaporation, precipitation, and runoff—has only been quantified at three points in time (1987, 2002, 2009). Due to this paucity of observations and large model biases, we cannot yet be sure how the Indian Ocean's freshwater cycle has responded to climate change, nor by how much it varies at seasonal and monthly time scales. To bridge this gap, we estimate the magnitude and variability of the Indian Ocean's freshwater budget using monthly varying oceanic data from May 2016 through April 2018. Freshwater converged into the basin with a mean rate and standard error of 0.35 ± 0.07 Sv (1 Sv ≡ $10^6$ $m^3$ $s^{-1}$), indicating that basinwide air–sea fluxes are net evaporative. This balance is maintained by salty waters leaving the basin via the Agulhas Current and fresher waters entering northward across the southern boundary and via the Indonesian Throughflow. For the first time, we quantify seasonal and monthly variability in Indian Ocean freshwater convergence to find amplitudes of 0.33 and 0.16 Sv, respectively, where monthly changes reflect variability in oceanic, rather than air–sea, fluxes. Compared with the range of previous estimates plus independent measurements from a reanalysis product, we conclude that the Indian Ocean has remained net evaporative since the 1980s, in contrast to long-term changes in its heat budget. When disentangling anthropogenic-driven changes, these observations of decadal and intra-annual natural variability should be taken into account.

KEYWORDS: Ocean; Indian Ocean; Atmosphere-ocean interaction; Ocean circulation; Freshwater

## 1. Introduction

Observations of global ocean salinity patterns over the past 50 years have revealed an intensifying freshwater cycle, whereby wet regions have become wetter and dry regions drier (e.g., Durack et al. 2012; Yu et al. 2020). The Indian Ocean is characterized by heavy precipitation and runoff (i.e., freshwater gains) in its monsoonal northeastern and central regions and by evaporative conditions (i.e., freshwater losses) toward the south. More frequent extreme positive Indian Ocean dipole events are already causing increased flooding in East Africa and droughts in Indonesia and Australia (Cai et al. 2014). Since the Indian Ocean has been warming faster than the Atlantic and Pacific over the last two decades, it may be an early indicator of how tropical–subtropical oceans and their freshwater cycles will respond to climate change, yet it remains the least observed of these basins (Beal et al. 2020; Ummenhofer et al. 2021).

Large-scale patterns in precipitation and evaporation influence the mean oceanic circulation which can be measured to infer air–sea freshwater fluxes (Lagerloef et al. 2010; Wijffels 2001). In the Indian Ocean, the Indonesian Throughflow (ITF) carries freshwater into the basin from the Pacific Ocean while salty water exits across its southern boundary, mostly via the Agulhas Current in the west, but also via the Leeuwin Current in the east. Over the past two decades several estimates of the freshwater budget of the Indian Ocean have been made using ship-based hydrographic (temperature, salinity, pressure) sections that cross the basin around latitude 32°S (Robbins and Toole 1997; Ganachaud et al. 2000; Bryden and Beal 2001; Sloyan and Rintoul 2001; Talley 2008; Hernández-Guerra and Talley 2016). These studies use volume-conserving inverse models over varying oceanic regions (Indian, Indo-Pacific, Southern, and global) to estimate absolute geostrophic transports and freshwater fluxes. All these studies have shown that the Indian Ocean is net evaporative, whereby approximately 0.4 Sv (1 Sv ≡ $10^6$ $m^3$ $s^{-1}$) of freshwater is lost to the atmosphere, on average. Most recently, Hernández-Guerra and Talley (2016) extended this observational record by using hydrographic sections from 2002 to 2009 to estimate freshwater convergences of 0.31 and 0.55 Sv, respectively. They suggested that the Indian Ocean may have become increasingly evaporative between 2002 and 2009.

Uncertainties around these freshwater convergences are large, not least because the inverse models are underconstrained. For example, all past studies, beginning with the seminal work of Toole and Warren (1993) but excluding Hernández-Guerra and Talley (2016), use the same hydrographic section collected in 1987, yet they yield estimates of net evaporation ranging from 0.2 to 0.6 Sv (Robbins and Toole 1997; Ganachaud et al. 2000; Bryden and Beal 2001; Sloyan and Rintoul 2001). In addition to these known uncertainties, the unknown variability in freshwater transport may be aliasing the handful of one-time sections.

Denotes content that is immediately available upon publication as open access.

*Corresponding author*: Kathryn L. Gunn, kathy.gunn@csiro.au, kgunn.sc@gmail.com

DOI: 10.1175/JPO-D-22-0057.1

© 2022 American Meteorological Society. For information regarding reuse of this content and general copyright information, consult the AMS Copyright Policy (www.ametsoc.org/PUBSReuseLicenses).

Brought to you by UNIVERSITY OF SOUTHAMPTON HIGHFIELD | Unauthenticated | Downloaded 11/08/23 03:00 PM UTC

Freshwater exchanges between the ocean and atmosphere are important to quantify because they dominate the freshwater cycle, thus influencing weather patterns (e.g., United Nations 2017; Hoegh-Guldberg et al. 2018). Yet, direct air–sea flux products for the Indian Ocean have large discrepancies that leave even the direction of the basinwide air–sea flux uncertain (Beal et al. 2020). At the same time, moored buoy observations [i.e., Research Moored Array for African–Asian–Australian Monsoon Analysis and Prediction (RAMA)] of air–sea fluxes do not capture the full expanse of the Indian Ocean and, most notably, leave gaps within boundary currents and upwelling systems that host some of the largest exchanges. Therefore, despite the uncertainties, oceanic data—like those we study here—provide an essential metric of the freshwater cycle (Schmitt 2008; Lagerloef et al. 2010).

Although the hydrographic section across the Indian Ocean at 32°S has not been reoccupied since 2009, with the maturation of the global Argo array it is possible to synthesize seasonal hydrographic cross sections of the upper 2000 m of the Indian Ocean using Argo profiles (McMonigal et al. 2018). Here, we combine these data with our observations from a moored array across the Agulhas Current at the western boundary (Gunn et al. 2020) to make new estimates of the Indian Ocean freshwater budget and, for the first time, attempt to constrain its decadal and intra-annual variability.

## 2. Data and methods

### a. Volume and salt transports

To determine the freshwater budget of the Indian Ocean we quantify the volume and salt transports flowing into and out of the basin. We define six components of the budget: Agulhas, Leeuwin, ITF, Ekman, upper interior (0–2000 m), and deep interior (>2000 m). For the Agulhas and upper interior components, we calculate the horizontal ($x$) and vertical ($z$) integrals of gridded velocity $v(x, z, t)$ and salinity $S(x, z, t)$ pairs from the moored array and mapped Argo observations (Figs. 1 and 2) as

$$T_{\text{flux}} = \int\int v dx dz \tag{1}$$

$$T_{\text{flux}} S_{\text{flux}} = \int\int vS\, dx dz. \tag{2}$$

These directly calculated volume ($T_{\text{flux}}$) and salt ($T_{\text{flux}}S_{\text{flux}}$) transports have units of Sv and Sv psu, respectively (McDonagh et al. 2015; Gunn et al. 2020, 2022). Positive values indicate flow into the basin and "flux" indicates the component of the budget. For the ITF, Leeuwin, deep interior, and Ekman components of the budget we use a volume transport and transport-weighted salinity (TWS) to estimate their salt transports as (Fig. 3):

$$T_{\text{flux}} S_{\text{flux}} = T_{\text{flux}} \times \text{TWS}. \tag{3}$$

The $T_{\text{flux}}$ and TWS for the ITF and Leeuwin Current are taken from the published literature (Gordon et al. 2010; Sprintall et al. 2009; Feng et al. 2003; Chen and Feng 2021). The Ekman salt transport is calculated using Ekman's theory, with observations of wind stress from ERA5 and TWS that is the average salinity over the upper 100 m of the mapped Argo data. For the unobserved deep interior, we derive an initial $T_{>2000}$ by conserving volume across all components of the budget using our best estimate of their 2010–19 mean volume transports (more details below). TWS for the deep interior is obtained by averaging all available ship-based salinities below 2000 m (Fig. 2c). We estimate a total error for each component by combining the transport- and salinity-derived errors following McDonagh et al. (2015) (see appendix). We calculate two sets of transports, the first representing a decadal mean state, 2010–19, which is required to provide an initial model for the time-varying circulation. The second set represents the Agulhas array period, 2016–18. This 2-yr period includes estimates of monthly-varying fluxes. The details of the calculations of each component are described next, including data sources and derived mean fluxes with uncertainties (see summaries in Tables 1 and 2 and error calculation in the appendix).

#### 1) Agulhas Current

The velocity and salinity fields of the Agulhas Current were measured continuously by moored instruments for a period of 24 months—from May 2016 through April 2018—as part of the Agulhas System Climate Array (ASCA; McMonigal et al. 2020; Gunn et al. 2020). The ASCA moorings were deployed in the same locations as those of the Agulhas Current Time series (ACT) experiment, which ran from 2010 to 2013 (Beal et al. 2015). The moorings were placed along an altimeter ground track, from the South African coastline at 33.30°S, 27.40°E to a location 300 km offshore at 35.75°S, 28.90°E. Using these data, we calculated the mean and standard error of Agulhas Current volume and salt transports to be −86.3 ± 11 Sv and −3025 ± 130 Sv psu, respectively (Gunn et al. 2020, 2022). To estimate a decadal mean for 2010–19, we combine these ASCA data (2016–18) with previous data from ACT (2010–13) to calculate a weighted-mean volume transport of −76.2 Sv (weighted by the length of each experiment). Combined with the 2016–18 mean TWS of 35.07 psu and Eq. (3), we estimate a decadal mean Agulhas Current salt transport of −2673 Sv psu.

#### 2) Leeuwin Current

The climatological mean volume transport and transport-weighted salinity of the Leeuwin Current, estimated from 50 years of sea level and hydrographic data near 32°S, are −3.4 Sv and 35.60 psu (Feng et al. 2003; Chen and Feng 2021). Feng et al. (2003) found that the annual average volume transport in El Niño, mean, and La Niña years is −3.0, −3.4, and −4.2 Sv, respectively, while Chen and Feng (2021) showed that salinity varies annually by up to 0.2 psu at 60 m depth. Therefore, we choose uncertainty estimates on these $T_{\text{flux}}$ and TWS values of 1.0 Sv and 0.2 psu (Table 2). Using Eq. (3), we find that the salt transport of the Leeuwin Current is −121 ± 35 Sv psu (Feng et al. 2003; Chen and Feng 2021). Lacking direct Leeuwin Current data for the period 2016–18

Brought to you by UNIVERSITY OF SOUTHAMPTON HIGHFIELD | Unauthenticated | Downloaded 11/08/23 03:00 PM UTC

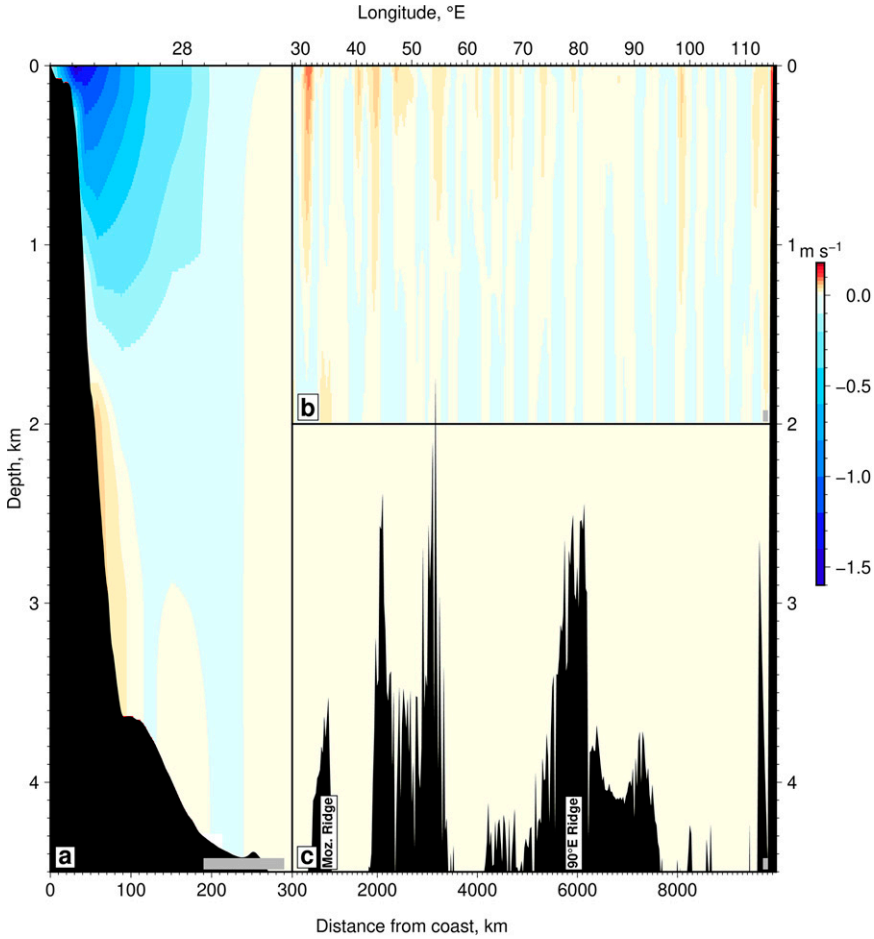


FIG. 1. The 2016–18 mean oceanic velocities (m $s^{-1}$) across southern boundary of Indian Ocean. The section extends between South Africa and Australia nominally along 36°S. (a) Agulhas Current. Direct velocities measured by ASCA moorings. (b) Upper interior. Absolute geostrophic velocities derived from optimally interpolated Argo profiles referenced to Argo drift velocities. (c) Deep interior. Uniform velocity of $6.5 \times 10^{-4}$ m $s^{-1}$, corresponding to 10 Sv of deep flow. Bathymetry shaded black with Mozambique and Ninety East ridges labeled. Gray bars in lower right are 100-km scales for each panel.

we use these same climatological volume and salt transports for both the decadal-mean and ASCA periods.

### 3) UPPER INTERIOR

The upper interior section is mapped across 36°S and joins the offshore ends of the Agulhas and Leeuwin Current sections. The volume and salt transports over the upper 2000 m are quantified monthly using geostrophic velocity and salinity fields from Argo float data. The Argo data are optimally mapped and combined with sea surface height measurements to suppress mesoscale variability (Willis and Fu 2008; Willis 2010; McMonigal et al. 2018). The absolute geostrophic velocity field is calculated using the thermal wind relation referenced to Argo drift velocities measured at 1000-m depth. The drift velocities are small and noisy, so we use mean drifts over the 2016–18 period and, for the decadal estimate, over the 2010–19 period. The resultant monthly fields have vertical and horizontal resolutions of 10 m and 0.25°, respectively (Figs. 2b and 3, dotted lines). We estimate uncertainties by comparing the geostrophic volume transport and section-mean salinity from the ship-based hydrographic section occupied in April 2009 (Swift and Becker 2021) with those derived from our mapped Argo/SSH data for the same month. The root-mean-square differences are 3.1 Sv and 0.04 psu. Finally, we calculate transports using Eqs. (1) and (2). The 2016–18 mean $T_{0\text{–}2000\text{m}}$ and uncertainty is 60.2 ± 3.1 Sv and mean $T_{0\text{–}2000\text{m}}S_{0\text{–}2000\text{m}}$ is 2108 ± 108 Sv psu. The decadal-mean upper interior volume transport, $T^{2010\text{–}19}_{0\text{–}2000\text{m}}$, is smaller at 50.8 Sv.

### 4) EKMAN LAYER

We calculate an Ekman transport using estimates of zonal wind stress along 36°S to add to the upper interior transport from Argo. We assume the Ekman layer is 100 m. Ekman

Brought to you by UNIVERSITY OF SOUTHAMPTON HIGHFIELD | Unauthenticated | Downloaded 11/08/23 03:00 PM UTC

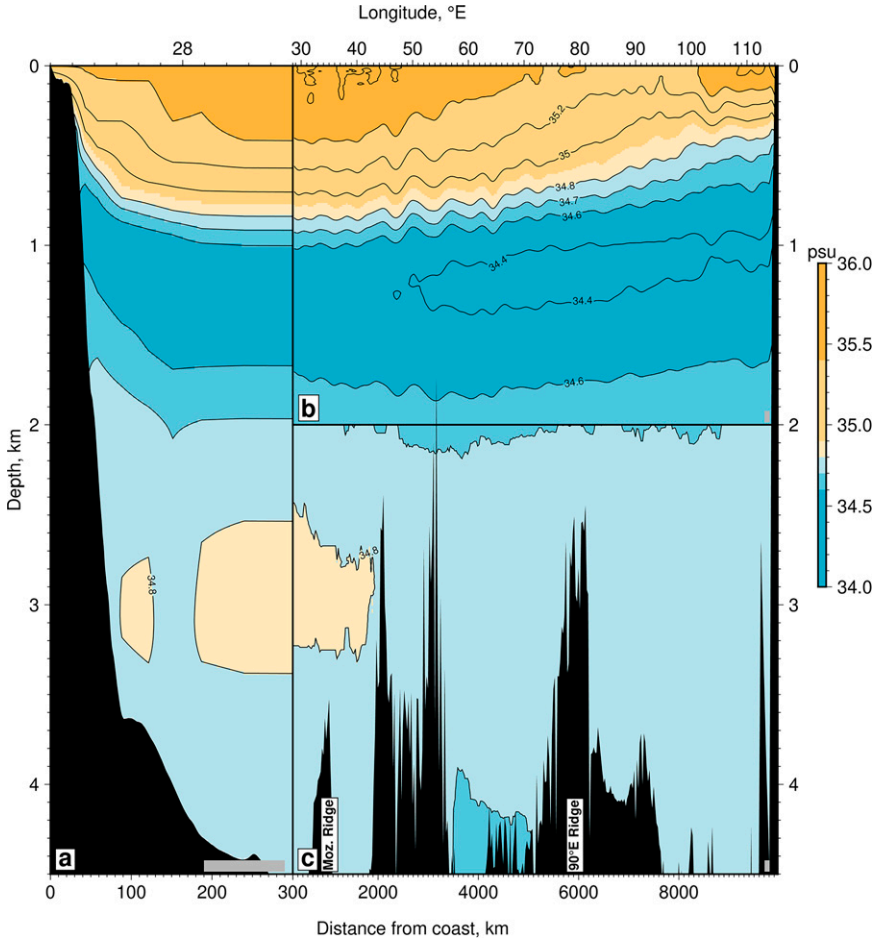


FIG. 2. 2016–18 mean salinities (psu) across southern boundary of Indian Ocean. The section extends between South Africa and Australia nominally along 36°S. (a) Agulhas Current. Salinity measured by the ASCA moorings. (b) Upper interior. Optimally interpolated salinity from Argo profiles. (c) Deep interior. Mean salinities from three ship-based occupations across south Indian Ocean in 1987, 2002, and 2009. Bathymetry shaded black with Mozambique and Ninety East ridges labeled. Gray bars in lower right are 100-km scales for each panel.

transports are calculated as $T_{\mathrm{Ekman}} = -\tau_x/\rho f$, where $\tau_x$ is the zonal wind stress taken from the ERA5 reanalysis product of the European Centre for Medium-Range Weather Forecasts (Hersbach et al. 2020) and $\rho$ is the mean density of seawater in the Ekman layer taken from mapped Argo fields. We use the monthly ERA5 wind stress at spatial resolutions of 0.25°. To estimate an uncertainty, we take the root-mean-square difference between NCEP and ERA5 derived Ekman transports, which is 1.0 Sv. The chosen Ekman layer depth has a negligible impact on the transport compared with this error of 1 Sv and we do not consider it further. For salinity, we use monthly means from the top 100 m of the mapped Argo fields and estimate an uncertainty of 0.05 psu based on the difference between these salinities and those calculated over the top 50 m. Finally, Ekman volume and salt transports, $T_{\mathrm{Ekman}}$ and $T_{\mathrm{Ekman}}S_{\mathrm{Ekman}}$, are calculated at monthly intervals [Eq. (3)]. In this way, we find the 2016–18 mean Ekman volume and salt transports are 4.5 ± 1 Sv and 162 ± 36 Sv psu, respectively. The decadal-mean volume transport of the Ekman layer, $T_{\mathrm{Ekman}}^{2010\text{–}19}$, is 4.2 Sv.

### 5) INDONESIAN THROUGHFLOW

For the Indonesian Throughflow we use a climatology of monthly varying volume transport and salinities that is based on observations from the International Nusantara Stratification and Transport (INSTANT) array (Gordon et al. 2010; Sprintall et al. 2009). TWS is taken to be the depth and horizontal mean salinity from the Makassar Strait moorings, and has a mean value of 34.57 psu, consistent with other estimates (Hernández-Guerra and Talley 2016; Gordon et al. 2019). To reflect the unknown magnitude of interannual variability of subsurface salinity at the connection between the Indian Ocean and Indonesian Sea, we use a salinity uncertainty of 0.2 psu (for more details see Gordon et al. 2019; Lee et al. 2019; Sprintall et al. 2019). Freshening of this amount has been observed downstream of the Indonesian Throughflow after strong

Brought to you by UNIVERSITY OF SOUTHAMPTON HIGHFIELD | Unauthenticated | Downloaded 11/08/23 03:00 PM UTC

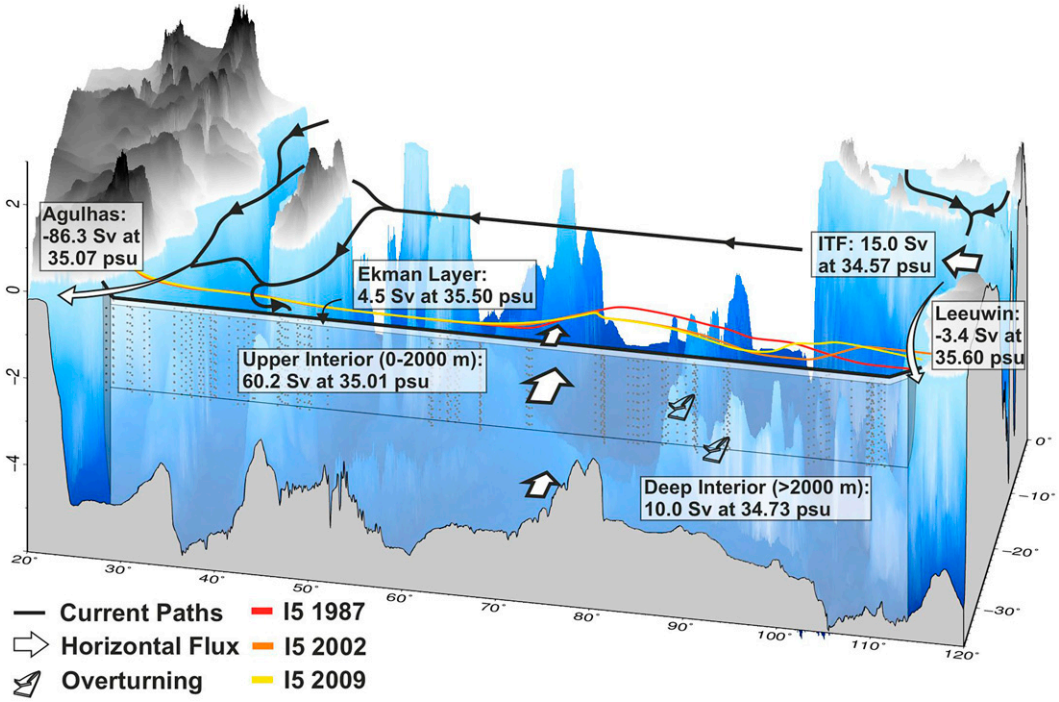


FIG. 3. The 2016–18 time mean components of Indian Ocean salt/freshwater budget. White arrows and text boxes describe direction and magnitude of each components volume transport and its transport-weighted salinity (positive values = transport into basin). Semi-transparent white shading highlights upper and deep interior sections along 36°S. Dotted lines show examples of Argo profiles mapped onto upper interior for month of June 2016. Blue and black shading is bathymetry and topography, respectively (Sandwell and Smith 2009). Curved arrows are a schematic indication of deep and shallow overturning cells.

La Niña events and is an example of significant interannual variability (e.g., Zhang et al. 2016). The volume transport of the Makassar Strait Throughflow, which represents over 70% of the total Indonesian Throughflow, has a standard deviation of about 4 Sv (Gordon et al. 2019), which we use as our uncertainty. The mean and uncertainties for volume and salt transport are 15 ± 4 Sv and 516 ± 140 Sv psu, respectively. We use these values for both the 2016–18 and decadal-mean estimates.

### 6) DEEP INTERIOR

The deep interior is the least observed component of the Indian Ocean. Three ship-based hydrographic sections collected along 32°S in 1987, 2002, and 2009 provide the only measurements of oceanic properties beneath 2000 m (Toole and Warren 1993; McDonagh et al. 2008; Hernández-Guerra and Talley 2016) for the interior southern boundary. From these, the sectional mean and standard deviation of salinity is 34.73 ± 0.03 psu and we use these values for the transport-weighted salinity and its uncertainty.

To determine a volume transport for the deep interior, we assume volume is conserved over the Indian Ocean during 2010–19 and calculate the residual of all the oceanic components detailed above plus an estimate of the decadal air–sea flux of freshwater ($T_{\mathrm{FW}}^{2010\text{–}19}$):

$$0 = T_{>2000\mathrm{m}}^{2010\text{–}19} + (T_{\mathrm{Agulhas}}^{2010\text{–}19} + T_{0-2000\mathrm{m}}^{2010\text{–}19} + T_{\mathrm{Ekman}}^{2010\text{–}19} + T_{\mathrm{Leeuwin}}^{2010\text{–}19} + T_{\mathrm{ITF}}^{2010\text{–}19} + T_{\mathrm{FW}}^{2010\text{–}19}),$$

where $T_{>2000\mathrm{m}}^{2010\text{–}19}$ is an estimate of the decadal mean volume transport of the deep interior. For $T_{\mathrm{FW}}^{2010\text{–}19}$ we use the mean of all previously published estimates derived from oceanic data. These range from 0.2 to 0.6 Sv and have a mean of 0.4 Sv (Toole and Raymer 1985; Wijffels et al. 1992; Robbins and Toole 1997; Ganachaud and Wunsch 2000; Bryden et al. 2005; Talley 2008; Hernández-Guerra and Talley 2016). All estimates indicate net evaporation, with volume lost from the basin on average, so that $T_{\mathrm{FW}}^{2010\text{–}19}$ is negative. Then, using the values listed previously, $T_{>2000\mathrm{m}}^{2010\text{–}19}$ is

$$T_{>2000\mathrm{m}}^{2010\text{–}19} = -1 \times (-76.2 + 50.8 + 4.2 - 3.4 + 15.0 - 0.40),$$

and is 10 Sv northward into the basin.

This estimate is similar to the estimates of McDonagh et al. (2008) and Hernández-Guerra and Talley (2016), who found $T_{>2000\mathrm{m}}$ between 7 and 11 Sv using the 2002 and 2009 transects, but is smaller than estimates by Robbins and Toole (1997) and Toole and Warren (1993), who found $T_{>2000\mathrm{m}}$ between 14 and 20 Sv using the 1987 transect. We consider the

Brought to you by UNIVERSITY OF SOUTHAMPTON HIGHFIELD | Unauthenticated | Downloaded 11/08/23 03:00 PM UTC

TABLE 1. The 2016–18 mean and standard deviation of transport-weighted salinity (TWS), volume ($T_{flux}$) and salt transports ($T_{flux}S_{flux}$), and freshwater convergence ($T_{FW}$). Total uncertainty for 2016–18 mean $T_{FW}$ also shown in parentheses in bottom row (see Table 2 for more information).

| | Budget component | TWS (psu) | $T_{flux}$ [Eq. (1)] (Sv) | $T_{flux}S_{flux}$ [Eq. (2)] (Sv psu) |
|---|---|---|---|---|
| Southern section | Ekman layer | 35.50 and 0.15 | 4.5 and 3 | 162 and 96 |
| | Upper interior (0–2000 m) | 35.01 and 0.15 | 60.2 and 7 | 2108 and 250 |
| | Deep interior (>2000 m) | 34.73 and 0.03 | 10.0 and 8 | 347 and 264 |
| | Leeuwin Current | 35.60 and 0 | −3.4 and 0 | −121 and 0 |
| | Agulhas Current | 35.07 and 0.07 | −86.3 and 14 | −3025 and 478 |
| Eastern section | ITF | 34.57 and 0.02 | 15.0 and 2 | 516 and 67 |
| | Freshwater convergence [$T_{FW}$; Eq. (6)] | | | 0.35 and 0.16 (±0.07) |

2002 and 2009 datasets to be more reliable. These more recent transects avoid a long section of shallow topography along the top of the southwest Indian Ridge and reveal that overturning in the Indian Ocean is double-celled: a deep cell with incoming Antarctic Bottom Water and outgoing Indian Deep Water, and an upper cell with incoming Subantarctic Mode Waters (including Antarctic Intermediate Water) and outgoing tropical–subtropical waters. This double-celled overturning circulation reduces the implied diffusivity, which was found to be twice as large as in the Atlantic or Pacific when assuming a single overturn (Lumpkin and Speer 2007). Nevertheless, to reflect the large uncertainty associated with the lack of data in the deep interior we estimate an error of 10 Sv, based on the full range of published estimates (3–20 Sv; Robbins and Toole 1997; Toole and Warren 1993; Sloyan and Rintoul 2001; Bryden and Beal 2001; McDonagh et al. 2008; Hernández-Guerra and Talley 2016).

### b. *Calculating freshwater convergence over the Indian Ocean*

The conservation of mass, or equivalently volume (Wijffels et al. 1992; McDonagh et al. 2008), and salt can be invoked to derive the freshwater convergence over the Indian Ocean (Knudsen 1900; Burchard et al. 2018; Schauer and Losch 2019). As no salt is exchanged at the sea surface, precipitation and evaporation transport pure freshwater (i.e., volume) across the air–sea interface ($T_{FW}$). To compensate evaporation (i.e., volume loss at the air–sea interface), the same volume of water must enter the basin which will have a salinity $S_{in}$. At the same time, to compensate the additional salt, some water must exit the basin with $S_{out} > S_{in}$. For our Indian Ocean budget, the subscripts in and out correspond to the ITF and the southern boundary at 36°S, respectively, and the conservation equations can be written as

$$T_{FW} + T_{ITF} = T_{36S}, \tag{4}$$

$$T_{ITF}S_{ITF} = T_{36S}S_{36S} \tag{5}$$

The terms within the equations can be assessed using Eqs. (1)–(3). In keeping with the conservation of volume in the basin, we apply a barotropic correction to the geostrophic velocity field of the interior following Bryden and Beal (2001). This barotropic correction is applied month-to-month in both the upper and deep interiors, so that the geostrophic shear derived from the in situ measurements is preserved. The correction is small, $O(10^{-3})$ cm s$^{-1}$.

TABLE 2. Summary of error sources and calculated uncertainties (for more details see appendix); $\overline{T_{flux}}$ = 2016–18 time-mean volume transport; $\overline{S'}$ = 2016–18 time-mean salinity anomaly; $\sigma_T$ and $\sigma_S$ = volume transport and salinity uncertainties. Total uncertainty shown in final columns. Note that salt transport uncertainty (not shown) is the product of $\sigma_T$ and transport-weighted salinity for each flux which is not the same as total uncertainty in final column.

| Budget component | $\overline{T_{flux}}$ (Sv) | $\overline{S'}$ (psu) | $\sigma_T$ (Sv) | $\sigma_S$ (psu) | Transport-derived uncertainty (Sv psu) | Salinity-derived uncertainty (Sv psu) | Total uncertainty (Sv psu) |
|---|---|---|---|---|---|---|---|
| Ekman | 4.5 | 1.03 | 1.0 | 0.05 | 1.03 | 0.23 | 1.1 |
| Upper interior (0–2000 m) | 60.2 | 0.19 | 3.1 | 0.04 | 0.59 | 2.41 | 2.5 |
| Deep interior (>2000 m) | 10.0 | 0.16 | 10.0 | 0.03 | 1.60 | 0.30 | 1.6 |
| Leeuwin | −3.4 | 1.08 | 1.0 | 0.20 | 1.08 | −0.68 | 1.3 |
| Agulhas Current | −86.3 | 0.25 | 11 | 0.05 | 2.75 | −4.32 | 5.1 |
| Throughflow | 15.0 | −0.07 | 4.0 | 0.20 | −0.30 | 2.99 | 3.0 |
| Total uncertainty on each monthly estimate of $T_{FW}$ (Sv) | | | | | | | 0.20 |
| Total uncertainty for 2016–18 mean $T_{FW}$ (Sv) | | | | | | | 0.07 |

Brought to you by UNIVERSITY OF SOUTHAMPTON HIGHFIELD | Unauthenticated | Downloaded 11/08/23 03:00 PM UTC

From the conservation Eqs. (4) and (5) it follows that

$$T_{\mathrm{FW}} = \frac{T_{36\mathrm{S}} S_{\mathrm{ITF}} - T_{36\mathrm{S}} S_{36\mathrm{S}}}{S_{\mathrm{ITF}}}, \tag{6}$$

where

$$T_{36\mathrm{S}} = T_{\mathrm{Agulhas}} + T_{\mathrm{Leeuwin}} + T_{0-2000\mathrm{m}} + T_{>2000\mathrm{m}} + T_{\mathrm{Ekman}} \quad \text{and}$$

$$T_{36\mathrm{S}} S_{36\mathrm{S}} = T_{\mathrm{Agulhas}} S_{\mathrm{Agulhas}} + T_{\mathrm{Leeuwin}} S_{\mathrm{Leeuwin}} + T_{0-2000\mathrm{m}} S_{0-2000\mathrm{m}} + T_{>2000\mathrm{m}} S_{>2000\mathrm{m}} + T_{\mathrm{Ekman}} S_{\mathrm{Ekman}}.$$

Positive values of $T_{\mathrm{FW}}$ indicate a convergence of freshwater into the basin and net evaporative conditions [note that Eq. (6) of this study is equivalent to Eq. (6) of Schauer and Losch (2019), Eq. (6.2.5) of Wijffels (2001), and Eq. (4) of McDonagh et al. (2015) in the mean].

For the period of the ASCA observations from May 2016 to April 2018 we can calculate how the freshwater budget changes from month to month using Eqs. (1), (2)/(3), and (6). For the first time, we estimate the amplitude of seasonal and monthly variability in freshwater convergence.

### c. *Decomposing the freshwater budget*

We investigate the drivers of freshwater convergence and its variability by decomposing the budget in several ways. First, we consider monthly air–sea freshwater fluxes based on atmospheric reanalysis estimates of evaporation, precipitation, and runoff, and compare these to our derivation of freshwater convergence from the oceanic data. Second, we separate the oceanic circulation into throughflow, gyre, and overturning circulations. Third, we examine the impact of seasonal and monthly changes in the salinities of the component oceanic fluxes on the overall freshwater budget.

We calculate net freshwater surface flux over the Indian Ocean—evaporation minus precipitation plus runoff ($E - P + R$)—using ERA5 (Hersbach et al. 2020). This product is available monthly at spatial resolutions of 1°. We used data from 1989 to 2019, smoothed over 5°, resampled at 1°, and integrated over the area of the Indian Ocean basin, including the Red and Persian Seas but excluding the South China and Indonesian Seas. Over the entire time period, the mean and standard deviation of $E - P + R$ are 0.46 and 0.28 Sv, respectively. Due to the large biases associated with evaporation, precipitation, and runoff estimate from reanalysis datasets (e.g., Hassler and Lauer 2021), we take the standard deviation of 0.28 Sv as the uncertainty of these data. The ERA5 $E - P + R$ provides an independent, monthly varying estimate of freshwater convergence for the period May 2016–April 2018, as well as decadal estimates of air–sea freshwater fluxes.

The freshwater transport across 36°S can be separated into three components that reflect different drivers of the ocean circulation, following Bryden and Beal (2001). The throughflow freshwater flux $F_T$ is related to the strength of the ITF. The overturning freshwater flux $F_O$ is related to the vertical exchange of water that is primarily driven by buoyancy fluxes and mixing. And the gyre freshwater flux $F_G$ is related to the horizontal gyre circulation that is driven by the wind. We first combine and remap velocity and salinity measurements from the Argo, WOCE, ASCA, and Leeuwin Current into a gridded dataset sampled every 500 m and 20 dbar. By doing so we can decompose the velocity and salinity fields across 36°S as follows:

$$v(x,z,t) = \overline{v}(t) + \langle v \rangle(z,t) + v'(x,z,t), \tag{7}$$

$$S(x,z,t) = \overline{S}(t) + \langle S \rangle(z,t) + S'(x,z,t), \tag{8}$$

where the overbar denotes a west-to-east, surface-to-seabed (i.e., vertical and horizontal) average, the angle brackets denote zonal averages of the deviation from the basinwide average, and the prime denotes residual deviations from the zonal average (Bryden et al. 2005; McDonagh et al. 2015). After this decomposition, the throughflow, overturning, and gyre freshwater transports are calculated as

$$F_T = -\frac{1}{S_{36\mathrm{S}}} T_{\mathrm{ITF}} (S_{\mathrm{ITF}} - S_{36\mathrm{S}}), \tag{9}$$

$$F_O = -\frac{1}{S_{36\mathrm{S}}} \int T_{\mathrm{pud}} [\langle v \rangle(z,t)][\langle S \rangle(z,t)]\, dz, \tag{10}$$

$$F_G = -\frac{1}{S_{36\mathrm{S}}} \int\int [v'(x,z,t)][S'(x,z,t)]\, dx\, dz, \tag{11}$$

respectively, where $T_{\mathrm{pud}}$ is the transport per unit depth given by $\int \langle v \rangle(z,t)\, dx$ and $S_{36\mathrm{S}} = 34.76$ psu is the time-mean, section-average salinity across the basin at 36°S.

For our final analysis we estimate the magnitude of changes in the freshwater budget that could be driven by changes in salinity alone, following McDonagh et al. (2015). To do this, we hold the volume transport of each component steady and allow only their transport-weighted salinities to change. We set the volume transports at their mean 2016–18 values, $\overline{T_{\mathrm{flux}}^{2016-18}}$, while TWS varies monthly according to the ASCA, Argo, and Makassar Strait salinity observations for the Agulhas, upper interior, and ITF component fluxes, respectively:

$$T_{\mathrm{flux}}^{\mathrm{FW}} = \frac{1}{S_{36\mathrm{S}}} \overline{T_{\mathrm{flux}}^{2016-18}} (\mathrm{TWS} - S_{36\mathrm{S}}). \tag{12}$$

By keeping volume transport constant, the variability of $T_{\mathrm{flux}}^{\mathrm{FW}}$ can be interpreted as a measure of change in freshwater transport caused by changes in the distribution of salinity within each component flux. Consider that each flux consists of a number of water masses, with differing salinities that can combine in several of ways to create the calculated volume and salt transports presented here. Note that these component freshwater fluxes are in the opposite direction to the component volume and salt transports when TWS $> S_{36\mathrm{S}}$. For example, the Agulhas Current's southward volume and salt transports are equivalent to a positive $T_{\mathrm{Agulhas}}^{\mathrm{FW}}$, because the export of salty water by the Agulhas Current is equivalent to a freshening of the basin and thus a positive freshwater flux.

Brought to you by UNIVERSITY OF SOUTHAMPTON HIGHFIELD | Unauthenticated | Downloaded 11/08/23 03:00 PM UTC

We assess the relative importance of these various drivers by calculating the correlation (expressed as Pearson's correlation coefficient, $r$) between each monthly time series and the total freshwater convergence $T_{FW}$ that we derived from our oceanic budget.

## 3. Results

### a. Indian Ocean freshwater budget

#### 1) 2016–18 MEAN

The 2016–18 mean velocity and salinity fields that represent the Indian Ocean along its southern boundary of 36°S are shown in Figs. 1 and 2. Flow in the Agulhas Current is relatively deep and broad during the 2016–18 period and as a result its transport is anomalously high at −86.3 Sv compared to the 25-yr proxy mean of about 76 Sv (Beal and Elipot 2016). There is southward flow throughout the water column save for a narrow, weak undercurrent over the continental slope (Beal and Bryden 1999; Beal et al. 2015). Flow in the upper interior is weak and disorganized, dominated by quasi-steady mesoscale features that have survived the mapping, eddy suppression, and averaging of the Argo dataset. The strongest northward flows in the interior are just outside the western boundary layer, to the west of the Mozambique Ridge at around 32°E, and at the eastern boundary in the Leeuwin Undercurrent (Fig. 1 and Schloesser 2014). The extremes in the salinity field are salty Subtropical Surface Waters that appear largely to the west of 70°E in the dynamical core of the gyre, and fresh Antarctic Intermediate Waters that enter the basin on the east side (Fig. 2). As a result, the Indian Ocean's freshwater budget is dominated by a southward flow of salty waters in the Agulhas Current and a northward flow of relatively fresher waters in the upper interior (Table 1).

The basinwide 2016–18 time mean components of Indian Ocean circulation and its salt/freshwater budget are summarized in Fig. 3. Southward transport of the Agulhas and Leeuwin Currents are −86.3 and −3.4 Sv, respectively. These southward flows are balanced by 60.2 Sv of northward transport across the upper interior and another 29.5 Sv composed of 4.5 Sv of northward Ekman transport, 15.0 Sv of flow into the Indian Ocean from the Pacific via the ITF, and a residual 10.0 Sv of northward deep interior flow (Figs. 3 and 4a). The Agulhas Current carries −3025 Sv psu of salt on average, and the upper interior carries 2108 Sv psu. The salt transports associated with the other flow components of the budget are an order of magnitude smaller (Fig. 4b and Table 1).

Together, these component salt transports reveal that freshwater converges into the Indian Ocean on average and indicates that the basin is net evaporative (Fig. 4c). Between 2016 and 2018, the $T_{FW}$ time series has a mean of 0.35 Sv with a standard error of 0.07 Sv and a standard deviation of 0.16 Sv. This new estimate of $T_{FW}$ is comparable to earlier studies that found convergences between 0.2 and 0.6 Sv during November 1987, and March of 2002 and 2009, and that have a mean of 0.4 Sv (Robbins and Toole 1997; Ganachaud et al. 2000; Bryden and Beal 2001; Sloyan and Rintoul 2001; Talley 2008; Hernández-Guerra and Talley 2016).

#### 2) MONTHLY AND SEASONAL VARIABILITY

Monthly freshwater convergence over the Indian Ocean varies between −0.05 and 0.55 Sv, departing significantly from its 2016–18 mean (Fig. 4c). The standard deviation of this signal is 0.16 Sv which we take to be representative of magnitude of month-to-month variability in $T_{FW}$. The magnitude of the seasonal cycle is ~0.33 Sv, given by averaging the freshwater convergence time series with respect to month of year then finding the difference between its maximum and minimum values (Fig. 5, black line). The seasonality appears to be semiannual, with maxima in austral summer (December–January) and winter (July–August) and minima in April–June and September–October. While only 24 months of data are available from which to discern the seasonal cycle, the phasing of freshwater convergence in each year observed is similar (2016, 2017, and 2018; Fig. 5).

The magnitude of the seasonal cycle that we find here challenges previous assumptions that the seasonal signal in freshwater convergence can be considered negligible (Wijffels 2001). Yet, by examining earlier estimates of freshwater convergence in the context of the month in which the ship-based data were collected, we suggest that the spread in those estimates is not related to the seasonal cycle (Fig. 5). Instead, the poorly constrained inverse methodology and the resultant magnitude of the Agulhas Current, which has a large barotropic component opaque to hydrographic data and the geostrophic assumption, have been shown to strongly influence the budget (Bryden and Beal 2001). For our calculation of the budget we have measured the Agulhas velocity directly and we use Argo float drift velocities to reference geostrophic shear across the upper interior (McMonigal et al. 2020).

The large magnitude of seasonal and monthly variability also challenges previous conclusions that the Indian Ocean has become increasingly evaporative over time. Hernández-Guerra and Talley (2016) estimated freshwater convergences of 0.30 Sv in 2002 and 0.55 Sv in 2009, using ship-based transects both completed in March (Fig. 5, black circles). However, we do not find a trend in the overall basinwide freshwater budget and also find 0.30 and 0.55 Sv within the range of monthly estimates of $T_{FW}$.

### b. Drivers of variability in the freshwater budget

#### 1) SURFACE FRESHWATER FLUXES

Our mean estimate of freshwater convergence derived from oceanic measurements over the period 2016–18 is consistent with contemporaneous estimates of $E - P + R$ from ERA5 (Fig. 6a). This product yields a 2016–18 mean net evaporation over the Indian Ocean of 0.46 ± 0.28 Sv, compared to our estimate of 0.35 ± 0.07 Sv. The standard deviation is 0.27 Sv, which is comparable to the seasonal signal estimated here, although the correlation between $E - P + R$ and $T_{FW}$ at monthly time scales is low (Fig. 6a). The air–sea flux ERA5 product suggest an annual cycle of convergence over the basin, while the oceanic fluxes suggest a semiannual cycle. This discrepancy could be due to large uncertainties in the surface flux products over regions of the ocean with

Brought to you by UNIVERSITY OF SOUTHAMPTON HIGHFIELD | Unauthenticated | Downloaded 11/08/23 03:00 PM UTC

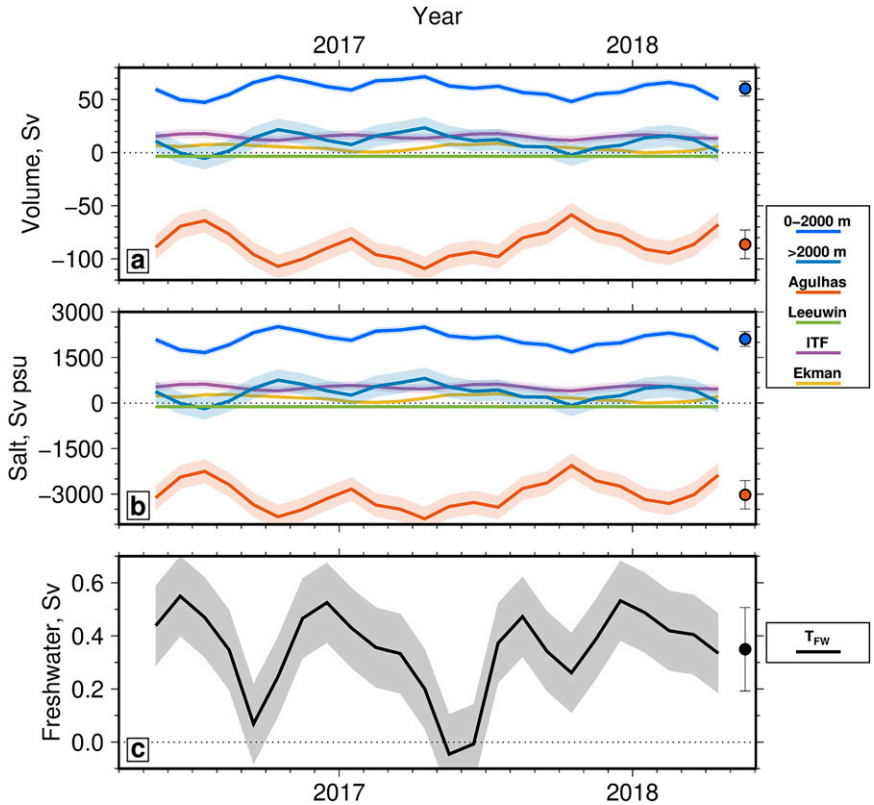


FIG. 4. Monthly time series of freshwater budget component transports. (a) Volume transport (Sv) of each component (colored lines) according to legend at right. Shading shows estimated uncertainty. Mean and standard deviation of upper interior transport (blue circle, 62 and 7 Sv) and Agulhas Current transport (red circle, −86 and 14 Sv). (b) As in (a), but salt transport (Sv psu) of each component. (c) Freshwater convergence, $T_{FW}$ (Sv), calculated from volume and salt transports in (a) and (b) using Eq. (6). Shading shows monthly uncertainty (0.15 Sv). Mean and standard deviation of freshwater convergence (black circle, 0.35 and 0.16 Sv). Positive values represent net evaporation.

strong mesoscale fronts and near boundaries. In the case of the Indian Ocean, large discrepancies remain between the surface flux products in these regions (Beal et al. 2020) and the western boundary is arguably better resolved by our oceanic dataset, which includes seven moorings of continuous observations to capture the Agulhas Current salt transport.

### 2) CIRCULATION

Separating the circulation at 36°S into gyre, overturning, and throughflow components we find that the overturning circulation is the largest contributor to Indian Ocean freshwater convergence, contributing 0.24 Sv on average (Fig. 6b). Perhaps counterintuitively, given the dominance of the Agulhas Current and upper interior in terms of salt transport, freshwater convergence resulting from the (full depth) horizontal gyre circulation is negligible in the mean. The dominance of overturning—a vertical exchange of salt in the Indian Ocean—reflects an export of salty subtropical surface waters via the Agulhas Current and an import of deeper fresh mode and intermediate waters across the interior. The mean sum of all circulation components, including the throughflow, is 0.35 Sv, equal to the total freshwater convergence.

At seasonal and monthly time scales, variability in freshwater convergence is not closely tied to changes in the strength of the circulation components ($r \leq 0.2$). The basin-wide freshwater convergence varies most closely with the throughflow component, but the correlation is not conclusive ($r = 0.2$) and the small magnitude of monthly variability in throughflow freshwater flux cannot account for the magnitude of the seasonal signal in freshwater convergence (Fig. 6b).

### 3) SALINITY VARIANCE

We explore the effect of salinity variance on the freshwater budget by allowing the transport-weighted salinity to vary month to month, while the volume transports of each flux are fixed [Eq. (12)]. The mean $T^{FW}_{flux}$ values indicate the relative strength and balance of the component parts of the freshwater budget and their summation is equal to $T_{FW}$; the freshwater budget is primarily a balance between an

Brought to you by UNIVERSITY OF SOUTHAMPTON HIGHFIELD | Unauthenticated | Downloaded 11/08/23 03:00 PM UTC

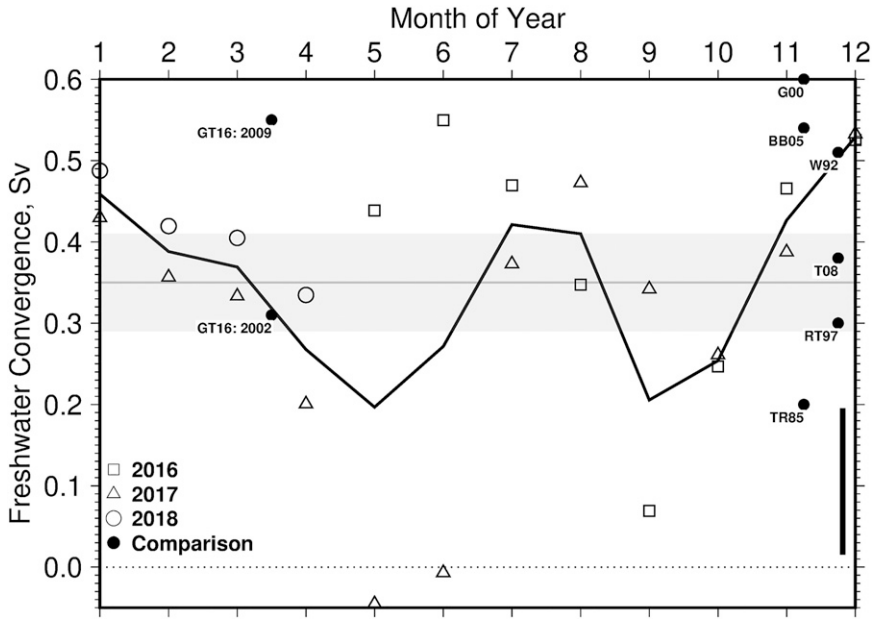


FIG. 5. Seasonal signal of freshwater convergence ($T_{FW}$). The thick black line shows monthly averages. White squares, triangles, and circles are estimates of $T_{FW}$ for each month in 2016, 2017, and 2018, respectively. The thin line with gray shading is the 2016–18 mean and standard error of $T_{FW}$ (0.35 ± 0.07 Sv). Black circles are previously published estimates of Indian Ocean freshwater convergence from ship-based hydrographic transects collected during November–December of 1987 and March–April of 2002 and 2009: T85 = Toole and Raymer (1985), W92 = Wijffels et al. (1992), R97 = Robbins and Toole (1997), G00 = Ganachaud and Wunsch (2000), BB05 = Bryden et al. (2005), T08 = Talley (2008), GT16 = Hernández-Guerra and Talley (2016). The thick black bar in lower right illustrates error of monthly $T_{FW}$ estimates (±0.20 Sv; see Table 2). Positive values represent freshwater convergence and net evaporation.

export of salty waters via the Agulhas Current, driving a mean freshwater transport of 0.70 Sv, and an import of salty waters (although not as salty as the Agulhas) across the upper interior, driving a mean freshwater transport of −0.43 Sv (Fig. 4c, red and blue lines). The $T_{ITF}^{FW}$ has a mean value of 0.08 Sv. The Ekman component, Leeuwin Current, and deep interior also have small freshwater fluxes of −0.09, 0.08, and 0.01 Sv, respectively (not shown). The sum of these 2-yr-averaged freshwater fluxes is 0.35 Sv.

The month-to-month changes in the component freshwater fluxes gives clues to the seasonal variability in the convergence of freshwater. We expected a large seasonal signal in $T_{ITF}^{FW}$, where sea surface salinity data from satellite shows fresher waters in the Indonesian Seas in boreal winter and spring due to monsoon precipitation and runoff (Lee et al. 2019; Hu and Sprintall 2017). The ITF salinity tendency, then, would be to enhance freshwater convergence over the Indian Ocean from December to May and reduce convergence in the remaining months of the year. However, the freshwater fluxes of the upper interior and Agulhas Current have far more influence on the total Indian Ocean freshwater convergence, with correlations of 0.7 and 0.4, respectively (Fig. 6c, blue and red lines). It is changes in salinity across the upper interior at 36°S that dominates month-to-month changes in basinwide freshwater convergence.

To better understand the origin of the seasonal signal in freshwater flux across the upper interior we look for regions where the temporal variance in both velocity and salinity are a maximum. We find these to be located at a longitudinal range of 28.5°–35°E, the western extreme of the interior (Fig. 7a). Following this we separate $T_{0-2000}^{FW}$ into two components representing (i) the center of the interior, 35°–90°E, and (ii) the western edge of the interior, 28.5°–35°E, to find that the edges of the interior drive almost all of the variability in freshwater convergence (Fig. 7b; $r = 0.8$).

## 4. Discussion

### a. Long-term trends in freshwater convergence

Despite intensification of the global freshwater cycle since the 1980s (e.g., Durack et al. 2012), we do not find a long-term trend in convergence of freshwater over the Indian Ocean over this time. The $E - P$ trends from 1950 to 2010 are positive in all the Southern Hemisphere subtropical gyres and the Indian Ocean is no exception. Between 10° and 30°S the Indian Ocean has become more evaporative (Skliris et al. 2014). On the other hand, the monsoonal Indian Ocean between 10°S and 20°N has become more precipitative associated with changes in the Southern Annular Mode (Huang et al. 2021). These regional analyses are

Brought to you by UNIVERSITY OF SOUTHAMPTON HIGHFIELD | Unauthenticated | Downloaded 11/08/23 03:00 PM UTC

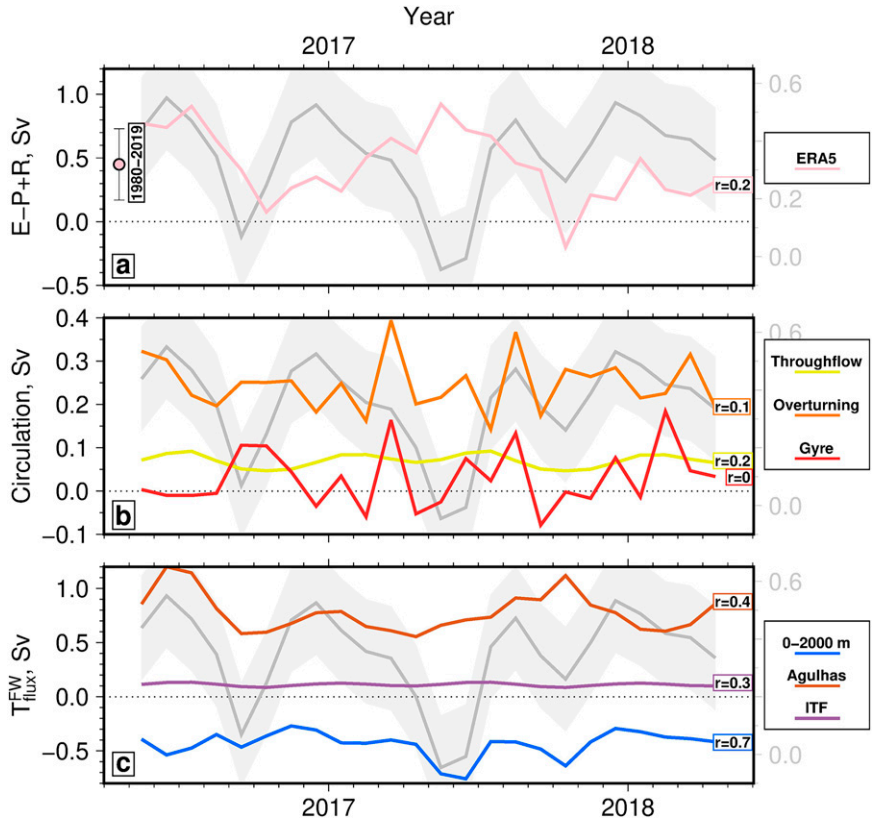


FIG. 6. Comparison of freshwater convergence time series with possible forcing mechanisms. (a) Comparison with surface freshwater fluxes. The pink line is the $E - P + R$ time series from ERA5. 1980–2019 mean and standard deviation (0.45 and 0.28 Sv) of $E - P + R$ shown on left-hand side. (b) Comparison with components that show strength variability of freshwater circulation. Yellow, orange, and red lines are freshwater circulation throughflow, overturning, and gyre components, respectively [Eq. (9)]. (c) Comparison with components that show salinity variability of freshwater circulation [Eq. (12)]. Blue, red, and purple lines are freshwater transport for upper interior (0–2000 m), Agulhas, and ITF fluxes, respectively. Volume is not conserved for this component, yet it still provides a useful indicator of salinity variability. Thick gray line with shading is the monthly $T_{FW}$ with error scaled to gray annotations on right-hand axis [Eq. (6)]. Values in colored boxes are Pearson correlation coefficient, $r$, of time series with $T_{FW}$.

consistent with the concept of wet regions becoming wetter and dry regions becoming drier. Instead of a basinwide trend in air–sea fluxes, we find significant natural variability balanced around a mean state of net evaporation; seasonal and monthly variability have amplitudes of 0.33 and 0.16 Sv, respectively, and the 2016–18 mean freshwater convergence is 0.35 Sv. Given the magnitude of the seasonal cycle and range of earlier oceanic freshwater estimates, we conclude that the mean freshwater convergence during 2016–18 is not significantly different from previous estimates in 1987, 2002, and 2009. This conclusion is further supported by independent decadal estimates of $E - P + R$ from ERA5. For 1980–89, 1990–99, 2000–09, and 2010–19 the decadal mean values of $E - P + R$ in the Indian Ocean are 0.38, 0.45, 0.51, and 0.45 Sv, respectively, showing no trend beyond the uncertainty of 0.28 Sv. Taken together, these results suggest that the basinwide freshwater budget of the Indian Ocean has remained unchanged since the late 1980s.

Given these results alongside evidence of an intensifying freshwater cycle, we conclude that a wetter northern Indian Ocean and a drier southern Indian Ocean largely cancel each other out when examined basinwide. It is important to note that strong interannual variability, especially in the Indonesian Throughflow (e.g., Lee et al. 2019; Gordon et al. 2019), would likely impact the freshwater budget in a given year. To quantify this variability, which is beyond the scope of the available observations, further analyses and continuation of high-quality data campaigns, such as ASCA and INSTANT, are needed.

Contrastingly, the heat budget of the Indian Ocean has responded dramatically to long-term climatic changes. The heat budget of the Indian Ocean has changed from divergent—the Indian Ocean drives the atmosphere—to neutral over the last two decades (McMonigal et al. 2022). Liu et al. (2021) point out that an enhanced hydrological cycle can increase oceanic

Brought to you by UNIVERSITY OF SOUTHAMPTON HIGHFIELD | Unauthenticated | Downloaded 11/08/23 03:00 PM UTC

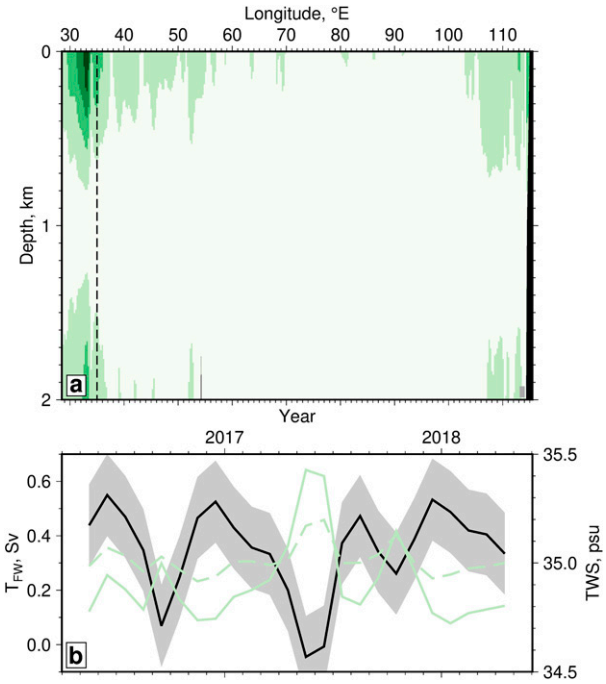


FIG. 7. (a) Temporal variance of velocity and salinity calculated as stdev($v \times S$). (b) Monthly comparison of $T_{FW}$ with transport-weighted salinity from different portions of interior. The black solid line is monthly mean of $T_{FW}$. The pale green dashed line is monthly mean of TWS across entire interior which has a $r < 0.5$ with $T_{FW}$. The pale green solid line is monthly mean of TWS from 28.5° to 35°E [highlighted by the dashed line in (a)], which has a $r > 0.8$ with $T_{FW}$.

heat uptake and moderate climate change. This effect may be significant in the Indian Ocean, where a rapid increase in upper-ocean heat content since the year 2000 contributed to the so-called hiatus in global warming (Li et al. 2018; Beal et al. 2020). On the other hand, several studies find that the ITF is largely responsible for rapid warming when considering the heat budget of the whole water column (Lee et al. 2015). McMonigal et al. (2022) used the same observations we use here to calculate their basinwide heat budget, finding that about two-thirds of the increase in heat content is due to the ITF and another one-third is related to a reduction in the amount of heat leaving the basin in the Agulhas Current, which has broadened (Beal and Elipot 2016). Using the same datasets, we find that although the freshwater cycle is intensifying, its basinwide magnitude has remained the same since 1980s. Taken together, these results suggest that the freshwater and heat budgets of the Indian Ocean respond differently to long-term climatic changes. Thus, when considering anthropogenic-driven long-term changes in the Indian Ocean freshwater budget, these observations of decadal and intra-annual natural variability should be taken into account.

### b. *Drivers of variability in the freshwater budget*

Oceanic convergence/divergence of freshwater is typically interpreted as a proxy of surface freshwater fluxes (e.g., Wijffels et al. 1992; Ganachaud 2003; Hernández-Guerra and Talley 2016), because ocean salinity is considered an integrator of changes in the water cycle, reflecting the exchange of freshwater between the ocean and the atmosphere. The upper 300–400 m of the salinity field is hence often treated as a rain gauge that integrates higher frequency $E - P + R$ fluxes (Schmitt 2008). While this correspondence bears out on average, according to our analysis it does not hold on monthly time scales. We find that seasonal signals of freshwater convergence do not correspond to independent monthly surface flux measurements of $E - P + R$. Instead, month-to-month changes in freshwater convergence follow changes in oceanic fluxes.

The dominance of advective, rather than surface, freshwater fluxes has been noted before in the Indian Ocean. Hu et al. (2019) concluded that oceanic advection of freshwater dominates basinwide salinity variability over the upper 400 m of the water column at interannual and decadal time scales. This is not the case in the northern Indian Ocean, however, where surface and advective freshwater fluxes have more or less equal importance in the freshwater budget (Trott et al. 2019). Therefore, it would seem that advective processes in the southern Indian Ocean dominate the basinwide freshwater budget.

Hu et al. (2019) showed that, of all the oceanic advective flux components, it is the ITF that drives variability in the Indian Ocean freshwater budget at interannual and decadal time scales. The ITF also drives variability in heat content and sea level at these time scales (Volkov et al. 2020). For example, between 2005 and 2013 the upper 400 m of the Indian Ocean freshened, while between 2014 and 2019 this trend reversed, and the water column became saltier (Nie et al. 2020). These interannual changes are associated with El Niño–Southern Oscillation. During La Niña there is an increase in rainfall over the Indonesian Seas and therefore a freshening (and strengthening) of the advective flux entering the Indian Ocean via the ITF (Hu and Sprintall 2017; Nie et al. 2020).

Here we show that at intra-annual time scales the ITF does not drive the freshwater budget, in contrast to its dominance at interannual and decadal time scales. This is despite an annual salinity signal in monsoon rainfall and runoff over the Indonesian Seas (Lee et al. 2019). Instead, we find a semiannual signal in $T_{FW}$ that is driven almost entirely ($r = 0.8$) by changes in advective salt fluxes at the western and, to a lesser extent, eastern reaches of the subtropical interior. We do not have a complete understanding of what drives these semiannual advective salt fluxes in the interior. However, it is likely that seasonal changes in gyre intensity and mode water formation both play a role. These same regions in the western and eastern interior dominate seasonal variability in the volume transport of the interior (McMonigal et al. 2018). And they lie just north of where mode waters are formed during austral winter (Olson et al. 1992; Sallée et al. 2006). We hypothesize the below two mechanisms for the first and second freshwater convergence minima.

The autumnal minimum may be driven by the seasonal strength of the Agulhas Current. In the western interior we

Brought to you by UNIVERSITY OF SOUTHAMPTON HIGHFIELD | Unauthenticated | Downloaded 11/08/23 03:00 PM UTC

see a mean mesoscale northward flow of order 1000 m deep that sits offshore of the Agulhas Current and just to the west of the Mozambique Ridge (Fig. 1b). This is part of a baroclinic recirculation of waters that are detrained from the Agulhas Return Current as it meanders around the Agulhas Plateau. Here, strong cyclonic eddies are shed from the meander trough more often during austral autumn (Boebel et al. 2003), following an austral summer peak in the volume of water entering the retroflection via the Agulhas Current (Krug and Tournadre 2012; Beal and Elipot 2016). This autumnal increase in the northward flux just offshore of the Agulhas Current would inject more salty surface waters, modified in the retroflection region (Gordon et al. 1987; Olson et al. 1992), back into the Indian Ocean, consistent with the minimum in freshwater convergence we observe in May (Fig. 5). Further evidence for this seasonal recirculation feature comes from the work of McMonigal et al. (2018), who show an anticyclonic dynamic height anomaly at the western end of the upper interior in April–June that causes a peak in the northward interior transport during austral autumn.

The winter minimum may be driven by mode water formation. Each austral winter surface waters are convectively modified in the interior just north of the subtropical front, in the vicinity of the Agulhas retroflection in the southwest Indian Ocean (Olson et al. 1992) and also in the far southeastern Indian Ocean (Sallée et al. 2006). Mode waters are formed when density surfaces outcrop and water exposed to the atmosphere is cooled and mixed vertically. These mode waters are cooler and more saline in the near-surface layers than subtropical Indian Ocean waters. Combined with surface-intensified northward currents, these mode waters would cause a positive (into the basin) salt flux anomaly in austral winter–spring at the western and eastern ends of our section that would correspond to the signals we see in Fig. 7 and to the second minimum we observe in freshwater convergence during September–October (Fig. 5).

## 5. Summary

Using our measurements from the Agulhas System Climate Array together with data from the Argo program during 2016–18 and INSTANT, we quantify the variability of volume and salt transport for six fluxes, as well as their resultant freshwater convergence, into and out of the Indian Ocean (Figs. 1–4). Considering the 2016–18 mean value, which is representative of air–sea freshwater exchange, these data extend the observational record of $E - P$ in the Indian Ocean from the 1980s and 2000s into the 2010s. Using two years of data, we make the first estimate of monthly-varying freshwater convergence over the Indian Ocean (Fig. 5) and find that oceanic advective fluxes across the western portion of the interior drives the variability of the Indian Ocean freshwater budget at seasonal time scales (Figs. 6 and 7).

On average, the Indian Ocean converged freshwater at a rate of 0.35 ± 0.07 Sv from May 2016 to April 2018, signifying a net evaporative basin. This mean is consistent with decadal and monthly varying independent estimates based on air–sea flux products from ERA5 that have a time mean of 0.46 ± 0.28 Sv. Freshwater convergence has large seasonal and monthly signals with amplitudes of 0.33 Sv, about the same order as the mean, and 0.16 Sv, receptively. A semiannual signal appears to be driven by oceanic advection of salinity anomalies in the far western region of the upper interior Indian Ocean and is unrelated to surface freshwater fluxes. Taken together, we find no evidence for a long-term trend in freshwater convergence over the Indian Ocean, which has remained net evaporative since the 1980s. This is notwithstanding extreme regional changes of precipitation and evaporation across the basin, which we conclude must balance out on average.

*Acknowledgments.* This work was funded by NSF Award 1459543 as part of the Agulhas System Climate Array. We thank the crews of the R/S *Algoa* and S/A *Agulhas* as well as Bradley Blows and Nauti-Buoys for building the ASCA moorings and leading deck operations on deployment and recovery. We acknowledge the support of the South African Department of Science and Innovation and the National Research Foundation of South Africa through the South African Environmental Observation Network (SAEON), and the Department of Environment, Forestry and Fisheries (DEFF, Branch: Oceans and Coasts). Special thanks to Elaine McDonagh for her support of, and input to, this manuscript.

*Data availability statement.* These measurements were analyzed using MATLAB and its implementation of GSW TEOS-10 (github.com/TEOS-10/GSW-Matlab). Figures were prepared using Generic Mapping Tools (gmt.soest.hawaii.edu). Argo data were collected and made freely available by the International Argo Program and the national programs that contribute to it (argo.ucsd.edu, ocean-ops.org). The Argo Program is part of the Global Ocean Observing System. Drifter-Derived Climatology of Global Near-Surface Currents is available at aoml.noaa.gov/phod/gdp/mean_velocity.php (Laurindo et al. 2017). Bathymetry is from the Global Bathymetry and Elevation Digital Elevation Model (SRTM30_PLUS v8; eatlas.org.au). Monthly averaged data from ERA5 are located at cds.climate.copernicus.eu. Individual instrument records (current meters, microCATs, and CPIES) collected during ASCA are available at accession.nodc.noaa.gov/0209237 and accession.nodc.noaa.gov/0210643. Gridded temperature, salinity and velocity fields are available at beal-agulhas.rsmas.miami.edu/data-and-products.

## APPENDIX

### Derivation of Errors

Salt and freshwater flux errors are calculated by combining salinity- and transport-derived uncertainties following McDonagh et al. (2015). The errors are summarized in Table 2.

#### *a. Property-derived error*

The salinity-derived error is the product of the salinity uncertainty ($\sigma_S$) with the time-mean integrated volume transport ($\overline{T_{\text{flux}}}$). We estimate the property uncertainties as the sampling uncertainty, which is typically an order of magnitude larger than the instrument error (Gunn et al. 2020; McMonigal et al. 2020).

Brought to you by UNIVERSITY OF SOUTHAMPTON HIGHFIELD | Unauthenticated | Downloaded 11/08/23 03:00 PM UTC

### b. Transport-derived error

The transport-derived error is the product of volume transport uncertainty ($\sigma_T$) and salinity anomaly ($\overline{S'}$). The salinity anomaly $\overline{S'}$ is the 2016–18 time-mean salinity anomaly calculated as each region's transport-weighted salinity minus $S_{\mathrm{ITF}}$, which is the time-mean salinity of the ITF and is 34.57 psu. It is reasonable to use the salinity anomaly, since the uncertainties in salinity must be compensated across the basin (under the assumption that salt is conserved within the basin).

### c. Total error

These salinity- and transport-derived errors are assessed for each flux and combined in quadrature to produce an uncertainty for each monthly estimate of $T_S$. Dividing by $S_{\mathrm{ITF}}$ gives the uncertainty for freshwater transport (penultimate row Table 2). The uncertainty on the 2-yr mean is found by diving the total monthly error by the square root of the degrees of freedom, $N$. In this experiment, $N$ is found by dividing the length of the time series in days, 730, by the integral time scale, 90, also in days, giving $N = 8$. The estimated uncertainties are shown in Table 2.

## REFERENCES


Beal, L. M., and H. L. Bryden, 1999: The velocity and vorticity structure of the Agulhas Current at 32°S. *J. Geophys. Res.*, **104**, 5151–5176, https://doi.org/10.1029/1998JC900056.

——, and S. Elipot, 2016: Broadening not strengthening of the Agulhas Current since the early 1990s. *Nature*, **540**, 570–573, https://doi.org/10.1038/nature19853.

——, ——, A. Houk, and G. M. Leber, 2015: Capturing the transport variability of a Western boundary jet: Results from the Agulhas Current Time-Series Experiment (ACT). *J. Phys. Oceanogr.*, **45**, 1302–1324, https://doi.org/10.1175/JPO-D-14-0119.1.

——, and Coauthors, 2020: A road map to IndOOS-2: Better observations of the rapidly warming Indian Ocean. *Bull. Amer. Meteor. Soc.*, **101**, E1891–E1913, https://doi.org/10.1175/BAMS-D-19-0209.1.

Boebel, O., T. Rossby, J. Lutjeharms, W. Zenk, and C. Barron, 2003: Path and variability of the Agulhas Return Current. *Deep-Sea Res. II*, **50**, 35–56, https://doi.org/10.1016/S0967-0645(02)00377-6.

Bryden, H. L., and L. M. Beal, 2001: Role of the Agulhas Current in Indian Ocean circulation and associated heat and freshwater fluxes. *Deep-Sea Res. I*, **48**, 1821–1845, https://doi.org/10.1016/S0967-0637(00)00111-4.

——, ——, and L. M. Duncan, 2005: Structure and transport of the Agulhas current and its temporal variability. *J. Oceanogr.*, **61**, 479–492, https://doi.org/10.1007/s10872-005-0057-8.

Burchard, H., and Coauthors, 2018: The Knudsen theorem and the total exchange flow analysis framework applied to the Baltic Sea. *Prog. Oceanogr.*, **165**, 268–286, https://doi.org/10.1016/j.pocean.2018.04.004.

Cai, W., A. Santoso, G. Wang, E. Weller, L. Wu, K. Ashok, Y. Masumoto, and T. Yamagata, 2014: Increased frequency of extreme Indian Ocean Dipole events due to greenhouse warming. *Nature*, **510**, 254–258, https://doi.org/10.1038/nature13327.

Chen, M., and M. Feng, 2021: A long-term, gridded, subsurface physical oceanography dataset and average annual cycles derived from *in situ* measurements off the Western Australia coast during 2009–2020. *Data Brief*, **35**, 106812, https://doi.org/10.1016/j.dib.2021.106812.

Durack, P. J., S. E. Wijffels, and R. J. Matear, 2012: Ocean salinities reveal strong global water cycle intensification during 1950 to 2000. *Science*, **336**, 455–458, https://doi.org/10.1126/science.1212222.

Feng, M., G. Meyers, A. Pearce, and S. Wijffels, 2003: Annual and interannual variations of the Leeuwin current at 32°S. *J. Geophys. Res.*, **108**, 3355, https://doi.org/10.1029/2002JC001763.

Ganachaud, A., 2003: Large-scale mass transports, water mass formation, and diffusivities estimated from World Ocean Circulation Experiment (WOCE) hydrographic data. *J. Geophys. Res.*, **108**, 3213, https://doi.org/10.1029/2002JC001565.

——, and C. Wunsch, 2000: Improved estimates of global ocean circulation, heat transport and mixing from hydrographic data. *Nature*, **408**, 453–457, https://doi.org/10.1038/35044048.

——, ——, J. Marotzke, and J. Toole, 2000: Meridional overturning and large-scale circulation of the Indian Ocean. *J. Geophys. Res.*, **105**, 26 117–26 134, https://doi.org/10.1029/2000JC900122.

Gordon, A. L., J. R. E. Lutjeharms, and M. L. Grundlingh, 1987: Stratification and circulation at the Agulhas retroflection. *Deep-Sea Res.*, **34A**, 565–599, https://doi.org/10.1016/0198-0149(87)90006-9.

——, and Coauthors, 2010: The Indonesian Throughflow during 2004–2006 as observed by the instant program. *Dyn. Atmos. Oceans*, **50**, 115–128, https://doi.org/10.1016/j.dynatmoce.2009.12.002.

——, and Coauthors, 2019: Makassar strait throughflow seasonal and interannual variability: An overview. *J. Geophys. Res. Oceans*, **124**, 3724–3736, https://doi.org/10.1029/2018JC014502.

Gunn, K. L., L. M. Beal, S. Elipot, K. McMonigal, and A. Houk, 2020: Mixing of subtropical, central and intermediate waters driven by shifting and pulsing of the Agulhas Current. *J. Phys. Oceanogr.*, **50**, 3545–3560, https://doi.org/10.1175/JPO-D-20-0093.1.

——, ——, ——, ——, and ——, 2022: Corrigendum. *J. Phys. Oceanogr.*, **52**, 183–186, https://doi.org/10.1175/JPO-D-21-0172.1

Hassler, B., and A. Lauer, 2021: Comparison of reanalysis and observational precipitation datasets including ERA5 and WFDE5. *Atmosphere*, **12**, 1462, https://doi.org/10.3390/atmos12111462.

Hernández-Guerra, A., and L. D. Talley, 2016: Meridional overturning transports at 30S in the Indian and Pacific Oceans in 2002–2003 and 2009. *Prog. Oceanogr.*, **146**, 89–120, https://doi.org/10.1016/j.pocean.2016.06.005.

Hersbach, H., and Coauthors, 2020: The ERA5 global reanalysis. *Quart. J. Roy. Meteor. Soc.*, **146**, 1999–2049, https://doi.org/10.1002/qj.3803.

Hoegh-Guldberg, O., and Coauthors, 2018: Impacts of 1.5°C global warming on natural and human systems. *Global Warming of 1.5°C*, V. Masson-Delmotte et al., Eds, Cambridge University Press, 175–312, https://www.ipcc.ch/sr15/.

Hu, S., and J. Sprintall, 2017: Observed strengthening of interbasin exchange via the Indonesian seas due to rainfall intensification. *Geophys. Res. Lett.*, **44**, 1448–1456, https://doi.org/10.1002/2016GL072494.

——, and Coauthors, 2019: Interannual to decadal variability of upper-ocean salinity in the southern Indian Ocean and the role of the Indonesian Throughflow. *J. Climate*, **32**, 6403–6421, https://soi.org/10.1175/JCLI-D-19-0056.1.


Brought to you by UNIVERSITY OF SOUTHAMPTON HIGHFIELD | Unauthenticated | Downloaded 11/08/23 03:00 PM UTC

Huang, P.-W., Y.-F. Lin, and C.-R. Wu, 2021: Impact of the southern annular mode on extreme changes in Indian rainfall during the early 1990s. *Sci. Rep.*, **11**, 2798, https://doi.org/10.1038/s41598-021-82558-w.

Knudsen, M., 1900: Ein hydrographischer Lehrsatz. *Ann. Hydrogr. Marit. Meteor.*, **28**, 316–320.

Krug, M., and J. Tournadre, 2012: Satellite observations of an annual cycle in the Agulhas Current. *Geophys. Res. Lett.*, **39**, L15607, https://doi.org/10.1029/2012GL052335.

Lagerloef, G., R. Schmitt, J. Schanze, and H.-Y. Kao, 2010: The ocean and the global water cycle. *Oceanography*, **23**, 82–93, https://doi.org/10.5670/oceanog.2010.07.

Laurindo, L. C., A. J. Mariano, and R. Lumpkin, 2017: An improved near-surface velocity climatology for the global ocean from drifter observations. *Deep-Sea Res. I*, **9**, 73–92, https://doi.org/10.1016/j.dsr.2017.04.009.

Lee, S.-K., W. Park, M. O. Baringer, A. L. Gordon, B. Huber, and Y. Liu, 2015: Pacific origin of the abrupt increase in Indian Ocean heat content during the warming hiatus. *Nat. Geosci.*, **8**, 445–449, https://doi.org/10.1038/ngeo2438.

Lee, T., S. Fournier, A. L. Gordon, and J. Sprintall, 2019: Maritime continent water cycle regulates low-latitude chokepoint of global ocean circulation. *Nat. Commun.*, **10**, 2103, https://doi.org/10.1038/s41467-019-10109-z.

Li, Y., W. Han, A. Hu, G. A. Meehl, and F. Wang, 2018: Multidecadal changes of the upper Indian Ocean heat content during 1965–2016. *J. Climate*, **31**, 7863–7884, https://doi.org/10.1175/JCLI-D-18-0116.1.

Liu, M., G. Vecchi, B. Soden, W. Yang, and B. Zhang, 2021: Enhanced hydrological cycle increases ocean heat uptake and moderates transient climate change. *Nat. Climate Change*, **11**, 848–853, https://doi.org/10.1038/s41558-021-01152-0.

Lumpkin, R., and K. Speer, 2007: Global ocean meridional overturning. *J. Phys. Oceanogr.*, **37**, 2550–2562, https://doi.org/10.1175/JPO3130.1.

McDonagh, E. L., H. L. Bryden, B. A. King, and R. J. Sanders, 2008: The circulation of the Indian Ocean at 32°S. *Prog. Oceanogr.*, **79**, 20–36, https://doi.org/10.1016/j.pocean.2008.07.001.

——, and Coauthors, 2015: Continuous estimate of Atlantic oceanic freshwater flux at 26.5°N. *J. Climate*, **28**, 8888–8906, https://doi.org/10.1175/JCLI-D-14-00519.1.

McMonigal, K., L. M. Beal, and J. K. Willis, 2018: The seasonal cycle of the South Indian Ocean subtropical gyre circulation as revealed by Argo and satellite data. *Geophys. Res. Lett.*, **45**, 9034–9041, https://doi.org/10.1029/2018GL078420.

——, ——, S. Elipot, K. L. Gunn, J. Hermes, T. Morris, and A. Houk, 2020: The impact of meanders, deepening and broadening, and seasonality on Agulhas Current temperature variability. *J. Phys. Oceanogr.*, **50**, 3529–3544, https://doi.org/10.1175/JPO-D-20-0018.1.

——, K. L. Gunn, L. Beal, S. Elipot, and J. K. Willis, 2022: Reduction in meridional heat export contributes to recent Indian Ocean warming. *J. Phys. Oceanogr.*, **52**, 329–345, https://doi.org/10.1175/JPO-D-21-0085.1.

Nie, X., Z. Wei, and Y. Li, 2020: Decadal variability in salinity of the Indian Ocean subtropical underwater during the Argo period. *Geophys. Res. Lett.*, **47**, e2020GL089104, https://doi.org/10.1029/2020GL089104.

Olson, D. B., R. A. Fine, and A. L. Gordon, 1992: Convective modifications of water masses in the Agulhas. *Deep-Sea Res.*, **39A**, S163–S181, https://doi.org/10.1016/S0198-0149(11)80010-5.

Robbins, P. E., and J. M. Toole, 1997: The dissolved silica budget as a constraint on the meridional overturning circulation of the Indian Ocean. *Deep-Sea Res. I*, **44**, 001264, https://doi.org/10.1016/S0967-0637(96)00126-4.

Sallée, J.-B., N. Wienders, K. Speer, and R. Morrow, 2006: Formation of subantarctic mode water in the southeastern Indian Ocean. *Ocean Dyn.*, **56**, 525–542, https://doi.org/10.1007/s10236-005-0054-x.

Sandwell, D. T., and W. H. Smith, 2009: Global marine gravity from retracked Geosat and ERS-1 altimetry: Ridge segmentation versus spreading rate. *J. Geophys. Res.*, **114**, B01411, https://doi.org/10.1029/2008JB006008.

Schauer, U., and M. Losch, 2019: Freshwater in the ocean is not a useful parameter in climate research. *J. Phys. Oceanogr.*, **49**, 2309–2321, https://doi.org/10.1175/JPO-D-19-0102.1.

Schloesser, F., 2014: A dynamical model for the Leeuwin Undercurrent. *J. Phys. Oceanogr.*, **44**, 1798–1810, https://doi.org/10.1175/JPO-D-13-0226.1.

Schmitt, R. W., 2008: Salinity and the global water cycle. *Oceanography*, **21**, 12–19, https://doi.org/10.5670/oceanog.2008.63.

Skliris, N., R. Marsh, S. A. Josey, S. A. Good, C. Liu, and R. P. Allan, 2014: Salinity changes in the World Ocean since 1950 in relation to changing surface freshwater fluxes. *Climate Dyn.*, **43**, 709–736, https://doi.org/10.1007/s00382-014-2131-7.

Sloyan, B. M., and S. R. Rintoul, 2001: The Southern Ocean limb of the global deep overturning circulation. *J. Phys. Oceanogr.*, **31**, 143–173, https://doi.org/10.1175/1520-0485(2001)031<0143:TSOLOT>2.0.CO;2.

Sprintall, J., S. E. Wijffels, R. Molcard, and I. Jaya, 2009: Direct estimates of the Indonesian throughflow entering the Indian Ocean: 2004–2006. *J. Geophys. Res.*, **114**, C07001, https://doi.org/10.1029/2008JC005257.

——, and Coauthors, 2019: Detecting change in the Indonesian seas. *Front. Mar. Sci.*, **6**, 257, https://doi.org/10.3389/fmars.2019.00257.

Swift, J., and S. Becker, 2021: CTD data from Cruise 33RR20160321, exchange version. CCHDO, accessed July 2021, https://doi.org/10.7942/C2008W.

Talley, L. D., 2008: Freshwater transport estimates and the global overturning circulation: Shallow, deep and throughflow components. *Prog. Oceanogr.*, **78**, 257–303, https://doi.org/10.1016/j.pocean.2008.05.001.

Toole, J. M., and M. E. Raymer, 1985: Heat and fresh water budgets of the Indian Ocean—Revisited. *Deep-Sea Res. I*, **32**, 917–928, https://doi.org/10.1016/0198-0149(85)90036-6.

——, and B. A. Warren, 1993: A hydrographic section across the subtropical South Indian Ocean. *Deep-Sea Res. I*, **40**, 1973–2019, https://doi.org/10.1016/0967-0637(93)90042-2.

Trott, C. B., B. Subrahmanyam, V. S. Murty, and J. F. Shriver, 2019: Large-scale fresh and salt water exchanges in the Indian Ocean. *J. Geophys. Res.*, **124**, 6252–6269, https://doi.org/10.1029/2019JC015361.

Ummenhofer, C. C., S. A. Murty, J. Sprintall, T. Lee, and N. J. Abram, 2021: Heat and freshwater changes in the Indian Ocean region. *Natl. Rev.*, **2**, 525–541, https://doi.org/10.1038/s43017-021-00192-6.

United Nations, 2017: The ocean's role in the hydrological cycle. *The First Global Integrated Marine Assessment: World Ocean Assessment I*, Cambridge University Press, 91–104, https://doi.org/10.1017/9781108186148.007.

Volkov, D. L., S.-K. Lee, A. L. Gordon, and M. Rudko, 2020: Unprecedented reduction and quick recovery of the South Indian Ocean heat content and sea level in 2014–2018. *Sci. Adv.*, **6**, eabc1151, https://doi.org/10.1126/sciadv.abc1151.

Brought to you by UNIVERSITY OF SOUTHAMPTON HIGHFIELD | Unauthenticated | Downloaded 11/08/23 03:00 PM UTC

Wijffels, S. E., 2001: Ocean transport of fresh water. *Ocean Circulation and Climate: Observing and Modelling the Global Ocean*, G. Siedler, J. Church, and J. Gould, Eds., International Geophysics Series, Vol. 77, Elsevier, 475–488, https://doi.org/10.1016/S0074-6142(01)80135-2.

——, R. W. Schmitt, H. L. Bryden, and A. Stigebrandt, 1992: Transport of freshwater by the oceans. *J. Phys. Oceanogr.*, **22**, 155–162, https://doi.org/10.1175/1520-0485(1992)022<0155:TOFBTO>2.0.CO;2.

Willis, J. K., 2010: Can in situ floats and satellite altimeters detect long-term changes in Atlantic Ocean overturning? *Geophys. Res. Lett.*, **37**, L06602, https://doi.org/10.1029/2010GL042372.

——, and L. L. Fu, 2008: Combining altimeter and subsurface float data to estimate the time-averaged circulation in the upper ocean. *J. Geophys. Res.*, **113**, C12017, https://doi.org/10.1029/2007JC004690.

Yu, L., S. A. Josey, F. M. Bingham, and T. Lee, 2020: Intensification of the global water cycle and evidence from ocean salinity: a synthesis review. *Ann. N. Y. Acad. Sci.*, **1472**, 76–94, https://doi.org/10.1111/nyas.14354.

Zhang, N., M. Feng, Y. Du, J. Lan, and S. E. Wijffels, 2016: Seasonal and interannual variations of mixed layer salinity in the southeast tropical Indian Ocean. *J. Geophys. Res. Oceans*, **121**, 4716–4731, https://doi.org/10.1002/2016JC011854.

Brought to you by UNIVERSITY OF SOUTHAMPTON HIGHFIELD | Unauthenticated | Downloaded 11/08/23 03:00 PM UTC